

An updated analysis of radion-higgs mixing in the light of LHC data

Nishita Desai^a Ushoshi Maitra^b Biswarup Mukhopadhyaya^b

^aDepartment of Physics and Astronomy,
University College London, UK

^bRegional Centre for Accelerator-based Particle Physics
*Harish-Chandra Research Institute,
Chhatnag Road, Jhusi, Allahabad - 211 019, India*

E-mail: n.desai@ucl.ac.uk, ushoshi@hri.res.in, biswarup@hri.res.in

ABSTRACT:

We explore the constraints on the parameter space of a Randall-Sundrum warped geometry scenario, where a radion field arises out of the attempt to stabilise the radius of the extra compact spacelike dimension, using the most recent data from higgs searches at the Large Hadron Collider (LHC) and the Tevatron. We calculate contributions from both the scalar mass eigenstates arising from radion-higgs kinetic mixing in all important search channels. The most important channel to be affected is the decay via $WW^{(*)}$, where no invariant mass peak can discern the two distinct physical states. Improving upon the previous studies, we perform a full analysis in the $WW^{(*)}$ channel, taking into account the effect of various cuts and interference when the two scalar are closely spaced. We examine both cases where the experimentally discovered scalar is either 'higgs-like' or 'radion-like'. The implications of a relatively massive scalar decaying into a pair of 125 GeV scalars is also included. Based on a global analysis of the current data, including not only a single 125 GeV scalar but also another one with mass over the range 110 to 600 GeV, we obtain the up-to-date exclusion contours in the parameter space. Side by side, regions agreeing with the data within 68% and 95% confidence level based on a χ^2 -minimisation procedure, are also presented.

Contents

1	Introduction	1
2	The model and its parameters	3
2.1	The minimal Randall-Sundrum model and the radion	3
2.2	Radion-Higgs mixing	5
3	Strategy for analysis	8
3.1	The overall scheme	9
3.2	Allowed regions of the parameter space	11
3.3	Best fit contours	11
4	Results and discussions	12
4.1	Exclusion of the Parameter Space	14
4.2	Regions of best-fit with the data	16
5	Conclusions	18
6	Acknowledgements	19

1 Introduction

The announced discovery of a boson in the mass range 125-126 GeV, by both the ATLAS [1] and CMS [2] collaborations at the Large Hadron Collider (LHC) experiment, has naturally generated a lot of enthusiasm among particle physicists. As of now, the properties of the particle whose signature has been avowedly noticed are consistent with those of the Standard Model (SM) higgs boson. However, the present data also leave some scope for it being a scalar with a certain degree of non-standard behaviour. The analysis of such possibilities, both model-independently and on the basis of specific theoretical scenarios, has consumed rather substantial efforts in the recent months.

One scenario of particular interest in this context is one with a warped extra spacelike dimension. First proposed by Randall and Sundrum (RS), it has a non-factorizable geometry with an exponential warp factor [3]. Furthermore, the extra dimension is endowed with an S_1/Z_2 orbifold symmetry, with two 3-branes residing at the orbifold fixed points, the SM fields being confined to one of the branes (called the ‘visible brane’, at $y = r_c\pi$, where r_c is the radius of the compact dimension and y is the co-ordinate along that dimension). When the warp-factor in the exponent has a value of about 35, mass parameters of the order of the Planck scale in the ‘bulk’ get scaled down to the TeV scale on the visible branch, thus providing a spectacular explanation of the hierarchy between these two scales.

A bonus in the low-energy phenomenology of this model is the occurrence of TeV-scale Kaluza-Klein (KK) excitations of the spin-2 graviton on the visible brane, with coupling to the SM fields suppressed by the TeV scale [4–6]. The mass limit on the lowest excitation of the graviton in this scenario has already gone beyond 2 TeV (with certain assumptions on the model parameters) [7, 8]. However, another interesting and testable feature of this theory results from the mechanism introduced to stabilize the radius of the compact dimension, where the radius is envisioned as arising from the vacuum expectation value (vev) of a modular field. This field can be naturally given a vev by hypothesizing a brane-dependent potential for it, resulting in a physical field of geometrical origin, popularly called the radion field, with mass and vev around the electroweak scale, which couples to the trace of the energy-momentum tensor [9, 10]. Consistency with general covariance demands the addition of terms giving rise to mixing between the SM higgs and the radion [11–15]. Consequently, speculations have been made on whether the 125-126 GeV state, instead of being a pure SM higgs, could instead be the radion, or a mixture of the two.

A number of studies have already taken place in this direction, based on both the ‘pure radion’ and ‘radion-higgs mixing’ hypotheses [16–39]. In the present work, we perform a global analysis of the available data, assuming that both of the physical states arising from radion-higgs mixing contribute to the event rates in various channels. Using both the 2011 and 2012 data, we obtain the best fit points in terms of the parameters of the model. Furthermore, we obtain the 95% confidence level contours in the parameter space, which indicate the extent to which new physics can be accommodated in the light of the available results. Side by side, we identify the regions which are disallowed by data in one or more channels, as obtained from the published 95% C.L. exclusion limits on the signal strength, defined as $\mu = \sigma/\sigma_{SM}$, where σ is the predicted cross-section in the relevant channel for a specific combination of the model parameters, and σ_{SM} is the corresponding prediction for the SM higgs boson. The region that is left after such exclusion can be treated as one where the presence of a radion-like (higgs-like) scalar is compatible with the data as of now. A comparison of this region with the 95% C.L. contours around the best fit values of the parameters indicates the viability (or otherwise) of this particular new physics scenario.

Our work improves upon other recent studies based on LHC data [35–37, 39] in a number of ways. This is the first global analysis, following a χ^2 -minimisation procedure, of radion-higgs mixing, using the latest available data from 7 and 8 TeV LHC runs to obtain best fit parameters and significance contours. We include the possibility of an additional scalar mass eigenstate coexisting with the 125 GeV state, with both of them contributing to the final states looked for, subject to event selection criteria pertaining to the 125 GeV higgs. While it is unlikely that the contribution from the additional scalar will be confused with the signal of a 125 GeV scalar in the $\gamma\gamma$ and $ZZ^{(*)}$ final states (as the reconstructed invariant mass will point to two distinct resonances), it cannot *a priori* be ruled out for the $WW^{(*)}$ channel. The presence of two neutrinos in the di-lepton final state makes it impossible to reconstruct the mass of the parent particle and one would therefore expect some enhancement to the signal strength due to the extra contribution from the second state which must be estimated by simulating the effect of the selection cuts used by the corresponding experimental analyses. This makes the best-fit regions different from what

one finds with the assumptions that the entire contribution in every channel comes from one scalar resonance only.

Secondly, we also use the strategy of simulating the full cut-based analysis in restricting the allowed regions from the available upper limit on σ/σ_{SM} for an addition scalar with different mass, demanding not only (a) the extra contribution at 125 GeV be smaller than the current upper limit, but also (b) the combined contribution using cuts corresponding to the SM higgs search at the mass of the extra resonance be smaller than the upper limit at that mass. Again, this makes a difference mainly in the $WW^{(*)}$ channel. The contribution here (as also in the case of global fits) is the sum of those from two distinct mass eigenstates, so that the acceptance of the cuts does not factor out when taking the ratio to expected SM cross section.

Thirdly, we have taken into account the interference between processes mediated by radion-higgs mixed mass eigenstates whenever they are close to each other. And finally, we have explicitly included processes where a relatively heavy, radion(higgs)-dominated state decays into two higgs(radion)-dominated scalars at 125 GeV, each of which can go to the decay channels searched for. In a way, this leads to an additional production mechanism of the 125 GeV state, which we have felt should be included in a full analysis.

The presentation of our paper is as follows. We outline the RS model with higgs-radion mixing in the next section. The strategy of our analysis is described in section 3, while section 4 contains the numerical results. We summarise and conclude in section 5.

2 The model and its parameters

2.1 The minimal Randall-Sundrum model and the radion

In the minimal version of Randall-Sundrum (RS) model, one has an extra warped space-like compact dimension $y = r_c\phi$, where r_c is the radius of compactification. An S_1/Z_2 orbifolding is applied with a pair of 3-branes at the orbifold fixed points (at $\phi = 0$ and $\phi = \pi$). Gravity, propagating in the bulk, peaks at the first of these branes, usually called the Planck (hidden) brane (at $\phi = 0$), while the SM fields are confined to the visible brane (at $\phi = \pi$).¹

The action for the above configuration is given by [3]

$$\begin{aligned}
S &= S_{gravity} + S_v + S_h \\
S_{gravity} &= \int d^4x \int_{-\pi}^{\pi} d\phi \sqrt{-G} \{-\Lambda + 2M_5^3 R\} \\
S_v &= \int d^4x \sqrt{-g_v} \{\mathcal{L}_v - V_v\} \\
S_h &= \int d^4x \sqrt{-g_h} \{\mathcal{L}_h - V_h\}
\end{aligned} \tag{2.1}$$

where the subscripts v and h refer to the visible and hidden branes respectively, G is the determinant of the five dimensional metric G_{MN} and the metrics on the visible and hidden

¹While various modifications, including for example, gauge fields in the bulk have been considered [40–46], we have, however, confined ourselves to the minimal RS scenario.

branes are given by

$$g_{\mu\nu}^v(x^\mu) \equiv G_{\mu\nu}(x^\mu, \phi = \pi), g_{\mu\nu}^h(x^\mu) \equiv G_{\mu\nu}(x^\mu, \phi = 0) \quad (2.2)$$

the greek indices being representation of (1+3) dimensional coordinates on the visible (hidden) brane. M_5 is the 5-dimensional Planck mass and Λ is the bulk cosmological constant. V_v and V_h are the brane tensions of visible and hidden branes respectively.

The bulk metric obtained after solving Einstein's equations is then

$$ds^2 = e^{-2k|y|} \eta_{\mu\nu} dx^\mu dx^\nu - dy^2 \quad (2.3)$$

where $k = \sqrt{\frac{-\Lambda}{24M_5^3}}$ and

$$V_h = -V_v = 24M_5^3 k. \quad (2.4)$$

M_5 is related to the 4-dimensional Planck mass M_{Pl} by

$$M_{Pl}^2 = \frac{M_5^3}{k} [1 - e^{-2kr_c\pi}] \quad (2.5)$$

The 5-dimensional metric consists solely of mass parameters whose values are around the Planck scale. For the choice $kr_c \simeq 12$, which requires barely an order of disparity between the scales k and $1/r_c$, the mass parameters on the visible brane are suppressed with respect to the Planck scale by the exponential factor $e^{kr_c\pi} \simeq 10^{16}$, thus offering a rather appealing explanation of the hierarchy between the Planck and TeV scales. The Kaluza-Klein (KK) decomposition of the graviton on the visible brane leads to a discrete tower of states, with one massless graviton and a series of TeV-scale spin-2 particles. The massless graviton couples to all matter fields with strength $\sim 1/M_P$, while the corresponding couplings for the massive modes (in the TeV range) receive an exponential enhancement, thus opening up the possibility of observing signals of the massive gravitons in TeV-scale experiments [4–6]. Current experimental limits from the LHC rule out any mass for the lowest graviton excitation below 1.15(2.47) TeV for $k/M_P \leq 0.01(0.1)$ [7].

The radius of compactification r_c , was an input by hand in the original model, however, it can be given a dynamic origin by linking it to the vev of a ϕ -independent modulus field, $T(x)$, so that $r_c = \langle T \rangle$. We can define a new field

$$\varphi(x) = \Lambda_\varphi e^{-k(T(x)-r_c)\pi} \quad (2.6)$$

with its vev given by $\Lambda_\varphi = \sqrt{\frac{24M_5^3}{k}} e^{-k\pi r_c}$.

A vev for the modulus field can be dynamically generated if it has a potential. To generate the potential for $\varphi(x)$, a scalar field with bulk action is included along with interaction terms on the hidden and visible branes. The terms on the branes cause the scalar field to develop a ϕ -dependent vev. Inserting this solution into the bulk scalar action and integrating over ϕ yields an effective potential for $\varphi(x)$ of the form

$$V_\varphi(r_c) = k\epsilon v_h^2 + 4k e^{-4kr_c\pi} (v_v - v_h e^{-kr_c\pi})^2 (1 + \epsilon/4) - k\epsilon v_h e^{-(4+\epsilon)kr_c\pi} (2v_v - v_h e^{-kr_c\pi}) \quad (2.7)$$

where $\epsilon \simeq m^2/4k^2$

$$V(\varphi) = \frac{k^3}{144M_5^6} \varphi^4 (v_v - v_h (\frac{\varphi}{\Lambda_\varphi \exp(k\pi r_c)})^\epsilon), \quad (2.8)$$

where v_v and v_h are interaction terms on the visible and hidden branes respectively and by assumption $\epsilon \ll 1$. This new massive field φ is the radion field, where mass is obtained from $\frac{\partial^2 V(\varphi)}{\partial \varphi^2}$. Furthermore, one obtains the minimum of $V(\varphi)$ for $kr_c \approx 12$ for $\ln(\frac{v_v}{v_h}) \sim 1$.

The radion mass, m_φ , and the vev Λ_φ , constitute the set of free parameters of the theory in the radion sector, which now has the distinction of ‘naturally’ generating a TeV-scale vev on the visible brane. They have implications on particle phenomenology within the reach of the LHC. In particular, the radion mass may turn out to be a little below a TeV, thus making the detection of radion somewhat easier than that of the KK mode of the graviton [9, 10].

Integrating over the orbifold coordinates it can be shown that the radion field couples to the trace of energy-momentum tensor (T_ν^μ). The canonically normalized effective action is

$$S_\varphi = \int d^4x \sqrt{-g} \left[\frac{2M_5^3}{k} \left(1 - \frac{\varphi^2}{\Lambda_\varphi^2} e^{-2k\pi r_c}\right) R + \frac{1}{2} \partial_\mu \varphi \partial^\mu \varphi - V(\varphi) + \left(1 - \frac{\varphi}{\Lambda_\varphi}\right) T_\mu^\mu \right] \quad (2.9)$$

It should be noted that, while the radion has couplings that are very similar to those of the SM higgs, it has additional interaction with massless gauge boson (photon, gluon) pairs via the trace anomaly terms.

2.2 Radion-Higgs mixing

In addition to the above action, general covariance also allows a higgs-radion mixing term [11], parametrized by the dimensionless quantity ξ . Such a term couples the higgs field to the Ricci scalar of the induced metric (g_{ind}) on the visible brane

$$S = -\xi \int d^4x \sqrt{-g_{ind}} R(g_{ind}) H^\dagger H \quad (2.10)$$

where $H = [(v+h)/\sqrt{2}, 0]$ with $v = 246$ GeV

For phenomenological purpose, we are interested in terms in T_μ^μ , which are bilinear in the SM fields. Retaining such terms only, one has

$$T_\mu^\mu = T_\mu^{(1)\mu} + T_\mu^{(2)\mu} \quad (2.11)$$

with

$$\begin{aligned} T_\mu^{(1)\mu} &= 6\xi v \square h \\ T_\mu^{(2)\mu} &= (6\xi - 1) \partial_\mu h \partial^\mu h + 6\xi h \square h + 2m_h^2 h^2 + m_{ij} \bar{\psi}_i \psi_j - M_v^2 V_{A\mu} V_A^\mu \end{aligned} \quad (2.12)$$

$T_\mu^{(1)\mu}$ induces a kinetic mixing between φ and h . After shifting φ with respect to its vacuum expectation value Λ_φ we obtain

$$\mathcal{L} = -\frac{1}{2} \varphi (\square + m_\varphi^2) \varphi - \frac{1}{2} h (\square + m_h^2) h - 6\xi \frac{v}{\Lambda_\varphi} \varphi \square h \quad (2.13)$$

We confine our study to a region of the parameter space where the radion vev Λ_φ is well above the vev of the SM higgs. Besides, it is phenomenologically safe not to consider ξ with magnitude much above unity, since a large value may destabilise the geometry itself through back-reaction. Thus one can make the further approximation $6\xi\frac{v}{\Lambda_\varphi} \ll 1$. In this approximation, the kinetic energy terms acquire a canonical form under the basis transformation from (φ, h) to (φ', h') , such that

$$\begin{aligned}\varphi &= (\sin\theta - \sin\rho\cos\theta)h' + (\cos\theta + \sin\rho\sin\theta)\varphi' \\ h &= \cos\rho\cos\theta h' - \cos\rho\sin\theta\varphi'\end{aligned}\quad (2.14)$$

where

$$\tan\rho = 6\xi\frac{v}{\Lambda_\varphi}, \quad \tan 2\theta = \frac{2\sin\rho m_\varphi^2}{\cos^2\rho(m_\varphi^2 - m_h^2)}\quad (2.15)$$

and one ends up with the physical masses

$$m_{\varphi', h'}^2 = \frac{1}{2} \left[(1 + \sin^2\rho)m_\varphi^2 + \cos^2\rho m_h^2 \pm \sqrt{\cos^4\rho(m_\varphi^2 - m_h^2)^2 + 4\sin^2\rho m_\varphi^4} \right]\quad (2.16)$$

The interactions of φ' and h' with fermions (f) and massive gauge bosons (V) is given by

$$\mathcal{L}_1 = \frac{-1}{v} (m_{ij}\bar{\psi}_i\psi_j - M_v^2 V_{A\mu} V_A^\mu) (A_h h' + \frac{v}{\Lambda_\varphi} A_\varphi \varphi')\quad (2.17)$$

As has been mentioned above, the coupling of φ to a pair of gluons also includes the trace anomaly term. Taking it into account, the gluon-gluon couplings for both of the mass eigenstates are given by

$$\mathcal{L}_2 = \frac{-1}{v} \frac{\alpha_s}{16\pi} G_{\mu\nu} G^{\mu\nu} (B_h h' + \frac{v}{\Lambda_\varphi} B_\varphi \varphi')\quad (2.18)$$

while the corresponding Lagrangian for the photon is

$$\mathcal{L}_3 = \frac{-1}{v} \frac{\alpha_{EM}}{8\pi} F_{\mu\nu} F^{\mu\nu} (C_h h' + \frac{v}{\Lambda_\varphi} C_\varphi \varphi')\quad (2.19)$$

where

$$\begin{aligned}a_h^1 &= \frac{v}{\Lambda_\varphi} (\sin\theta - \sin\rho\cos\theta), \\ a_h^2 &= \cos\rho\cos\theta, \\ a_\varphi^1 &= \cos\theta + \sin\rho\sin\theta, \\ a_\varphi^2 &= \frac{\Lambda_\varphi}{v} (\cos\rho\sin\theta), \\ A_h &= a_h^1 + a_h^2, \\ A_\varphi &= a_\varphi^1 - a_\varphi^2,\end{aligned}$$

$$\begin{aligned}
B_h &= A_h F_{1/2}(\tau_t) - 2b_3 a_h^1, \\
B_\varphi &= A_\varphi F_{1/2}(\tau_t) - 2b_3 a_\varphi^1, \\
C_h &= A_h \left(\frac{4}{3} F_{1/2}(\tau_t) + F_1(\tau_W) \right) - (b_2 + b_Y) a_h^1, \\
C_\varphi &= A_\varphi \left(\frac{4}{3} F_{1/2}(\tau_t) + F_1(\tau_W) \right) - (b_2 + b_Y) a_\varphi^1, \\
\tau_t &= \frac{4m_t^2}{q^2}, \\
\tau_W &= \frac{4m_W^2}{q^2}, \\
b_3 &= 7, \quad b_2 = 19/6, \quad b_Y = -41/6.
\end{aligned} \tag{2.20}$$

where $q^2 = m_{h'}^2, (m_{\varphi'}^2)$ depending on $h'(\varphi') \rightarrow gg, \gamma\gamma$. b_2, b_3 and b_Y are the SM β -function coefficients in $SU(3)$ and $SU(2) \times U(1)_Y$ respectively. $F_1(\tau_W)$ and $F_{1/2}(\tau_t)$ are the form factor for W and top loop respectively. The form of these functions are

$$\begin{aligned}
F_{1/2}(\tau) &= -2\tau[1 + (1 - \tau)f(\tau)], \\
F_1(\tau) &= 2 + 3\tau + 3\tau(2 - \tau)f(\tau), \\
f(\tau) &= [\sin^{-1}(\frac{1}{\sqrt{\tau}})]^2, \quad \text{if } \tau \geq 1 \\
&= \frac{1}{4}[\ln(\frac{\eta_+}{\eta_-}) - i\pi]^2, \quad \text{if } \tau < 1 \\
\eta_{\pm} &= 1 \pm \sqrt{1 - \tau}.
\end{aligned} \tag{2.21}$$

The coupling of φ to h depends on the Goldberger-Wise stabilization potential $V(\varphi)$. On assuming the self-couplings of φ in $V(\varphi)$ to be small, we have

$$\Gamma(\varphi' \rightarrow h' h') = \frac{m_{\varphi'}^3}{32\pi\Lambda_\varphi^2} [1 - 6\xi + 2\frac{m_{h'}^2}{m_{\varphi'}^2} (1 + 6\xi)]^2 \sqrt{[1 - 4\frac{m_{h'}^2}{m_{\varphi'}^2}]} \tag{2.22}$$

Obviously, all interactions of either physical state are now functions of $m_{\varphi'}, m_{h'}, \Lambda_\varphi$ and ξ . In our subsequent calculations, we use these as the basic parameters, obtaining in each case the quantities m_φ, m_h by inverting (Eqn. 2.16). Requiring that the discriminant in (Eqn. 2.16) to remain positive implies a restriction on the parameter ξ as a function of the remaining three parameters. This constitutes a ‘‘theoretically allowed’’ region in ξ for given $(m_{h'}, m_{\varphi'}, \Lambda_\varphi)$. Within this region, we have two solutions corresponding to $m_\varphi > m_h$ and $m_\varphi < m_h$ in (Eqn. 2.16). In the first case we have $m_{\varphi'} \rightarrow m_\varphi$ and $m_{h'} \rightarrow m_h$ in the limit $\xi \rightarrow 0$. Exactly the opposite happens in the other case, with $m_{\varphi'} \rightarrow m_h$ and $m_{h'} \rightarrow m_\varphi$ as ξ approaches zero. A further constraint on ξ follows when one requires $m_\varphi > m_h$. This is because one has in that case,

$$m_\varphi^2 - m_h^2 = \frac{\sqrt{D} - \sin^2 \rho (m_{\varphi'}^2 + m_{h'}^2)}{1 - \sin^4 \rho} \tag{2.23}$$

where,

$$D = (m_{\varphi'}^2 + m_{h'}^2)^2 - 4(1 + \sin^2 \rho) m_{\varphi'}^2 m_{h'}^2 \tag{2.24}$$

One thus ends up with the condition $\sqrt{D} > \sin^2 \rho(m_\varphi^2 + m_{h'}^2)$, thus yielding an additional constraints on ξ .

In the other case described above one has

$$m_\varphi^2 - m_h^2 = -\frac{\sqrt{D} + \sin^2 \rho(m_\varphi^2 + m_{h'}^2)}{1 - \sin^4 \rho} \quad (2.25)$$

which trivially ensures $m_\varphi < m_h$.

We now define the convention for our analysis. (Eqn. 2.16) implies that the lightest state will always be h' . Thus, when $m_\varphi < m_h$, h' becomes the radion-dominated state i.e. $m_{h'} \rightarrow m_\varphi$ when $\xi \rightarrow 0$. On the other hand, when $m_\varphi > m_h$, we have $m_{h'} \rightarrow m_h$ when $\xi \rightarrow 0$. Let us label φ' (h') as the mixed radion state (R) if, on setting $\xi = 0$, one recovers $m_{\varphi'} = m_\varphi$ ($m_{h'} = m_\varphi$). The other state is named the mixed higgs state (H).

Basically, the two interchangeable limits of the states h' and φ' for $\xi = 0$ in the two cases arise from the fact that the angle θ in (Eqn. 2.15) is 0 or $\pi/2$, depending on whether $m_\varphi > m_h$ or $m_\varphi < m_h$. Both of the above mass inequalities are thus implicit in (Eqn. 2.16).

3 Strategy for analysis

We propose to scan over the parameter space in terms of masses of the observable physical eigenstates m_H and m_R for all allowed values of the mixing parameter ξ for a given Λ_φ . Since one scalar has been discovered at the LHC, two possibilities arise — viz. we identify the resonance near 125 GeV with either H or R . To cover both these, we present two scenarios based on the conventions defined in the previous section. In the first case, we will fix mass of the mixed higgs state ($m_H = 125$ GeV) and scan over the mass of the mixed radion state (m_R) from 110 to 600 GeV. Exactly the opposite is done in the other case. We describe our analysis using the first case with the understanding that the identical arguments apply when m_R is held fixed at 125 GeV. To improve the efficiency of our scan, we restrict it to two parameters viz. (m_R, ξ) and take snapshot values of Λ_φ at 1.5, 3, 5 and 10 TeV.

While it is possible to constrain Λ_φ further using either heuristic arguments or from searches for KK excitation of the RS graviton [47], we refrain from doing so to examine whether the current higgs search data can provide a complementary method for constraining the parameters of the RS model. Thus we start our study with the lowest value radion vev at 1.5 TeV. Taken together with the mass limits on the first excitation of the RS graviton, this might imply values of the bulk cosmological constant well into the trans-Planckian region where quantum gravity effects may in principle invalidate the classical RS solution. However, it may also be possible to reconcile a low radion vev with rather large graviton masses in some extended scenarios, such as one including a Gauss-Bonnet term in the 5-dimensional action [48–52].

We simulate the kinematics of the signal (higgs production and decay) using Pythia 8.160 [53] and reweighting according to the changed couplings. In the region where the second resonance lies between 122-127 GeV, we use Madgraph 5 [54] to calculate the full

cross section for $pp \rightarrow X \rightarrow WW^{(*)}/ZZ^{(*)}/\gamma\gamma$ to include interference from both states. The SM rates are taken from [55, 56].

3.1 The overall scheme

In this study, we ask two questions: first, what fraction of the radion-higgs mixing parameter space survives the observed exclusion limits on signal strengths in various search channels for the SM higgs; and second, if a radion-higgs scenario can explain the current data with a better fit than the SM?

Having framed these questions, we compare the theoretical predictions with observed data in various channels, namely, $\gamma\gamma$, $ZZ^{(*)} \rightarrow 4\ell$, $WW^{(*)} \rightarrow 2\ell + MET$, $b\bar{b}$ and $\tau\bar{\tau}$. Each channel receives contribution from both of the states H and R . Since the production channels for both H and R are same as the SM higgs (denoted henceforth as h_{SM}), albeit with modified couplings to SM particles, the production cross section of a given scalar can be written in terms of the SM higgs production cross section multiplied by a function of the modified couplings. We denote this function by $p_{mode}^{R,H}$, e.g. in the gluon-fusion mode,

$$p_{gg}^R(m) = \frac{\sigma(gg \rightarrow R)}{\sigma(gg \rightarrow h_{SM})} \Big|_{m_R=m_h=m} = \frac{B(R \rightarrow gg)}{B(h_{SM} \rightarrow gg)} \quad (3.1)$$

In general, we expect the acceptance of the cuts to depend on (a) the production mode, and (b) mass of the resonance. Let us denote the acceptance of cuts applied for a candidate mass m by the experimental analysis in a given channel as $a(m)_{prod-channel}$. Thus the predicted signal strength at a particular mass $\mu(m) = \sigma/\sigma_{SM}(m_{h_{SM}} = m)$ in any given decay channel c is given by

$$\mu(m; c) = \sum_{j=gg, VBF, VH} \left\{ p_j^H \frac{a(m; H)_j}{a(m; h_{SM})_j} \frac{B(H \rightarrow c)}{B(h_{SM} \rightarrow c)} + p_j^R \frac{a(m; R)_j}{a(m; h_{SM})_j} \frac{B(R \rightarrow c)}{B(h_{SM} \rightarrow c)} \right\} \quad (3.2)$$

In this analysis, we will be assuming that the state discovered at the LHC is the higgs-like H ($m_H = m_{h_{SM}} = 125$ GeV) for the first case and the radion like state R ($m_R = m_{h_{SM}} = 125$ GeV) for the second. Therefore, we expect the acceptances to cancel for one of the terms but not for the other where the second physical state has a different mass. For the rest of this section, we derive the formulae assuming the first case with the understanding that the expressions for the second case can be obtained merely by switching m_R and m_H .

For channels where the resonance is fully reconstructible viz. $\gamma\gamma$, $b\bar{b}$ and $ZZ^{(*)}$, the analyses use reconstructed mass to identify the resonance and therefore contribution from the second state are negligible if the resonance is narrow. Furthermore, by restricting the number of jets in the final state, it is possible to restrict contribution to the dominant production mode. Since the Lorentz structure of the couplings of R or H is the same as the SM higgs h_{SM} , the acceptances also factor out. Therefore, for $h + 0$ jets, in $\gamma\gamma$ and

$ZZ^{(*)}$ channels, $\mu = \sigma/\sigma_{SM}$ takes the simplified form

$$\mu(c) = p_{gg}^H \frac{B(H \rightarrow c)}{B(h_{SM} \rightarrow c)} = \frac{B(H \rightarrow c)B(H \rightarrow gg)}{B(h_{SM} \rightarrow c)B(h \rightarrow gg)} \quad (3.3)$$

However, in the $WW^{(*)}$ channel, the final state is not fully reconstructible and therefore we need to consider contributions from both the scalar physical states. Even on restricting to zero- and one-jet final states (which are largely due to gg fusion), we still have

$$\mu(m; WW) = p_{gg}^H \frac{a(m; H)}{a(m; h_{SM})} \frac{B(H \rightarrow WW)}{B(h_{SM} \rightarrow WW)} + p_{gg}^R \frac{a(m; R)}{a(m; h_{SM})} \frac{B(R \rightarrow WW)}{B(h_{SM} \rightarrow WW)} \quad (3.4)$$

The branching fraction $R \rightarrow WW^{(*)}$ reaches its maximal value when its mass passes the threshold $m_R = 2m_W$. At this point, the largest contribution to the dilepton final state can come from decay of R rather than H . Therefore, even with fixed mass of H at 125 GeV, the presence of another state that can contribute to the signature results in much stronger bounds on the radion-higgs mixed scenario. To estimate the effect of this, we have implemented the kinematical cuts on the leptons, jets and missing energy as described by the respective ATLAS [57] and CMS [58] analyses. We verify that our simulation of these analyses reproduce the expected number of signal events for a SM higgs within the errors quoted by the respective analyses.

In the $h+2$ jets channel, the requirement of two well-separated jets means the dominant contribution comes to VBF instead of gg fusion. However, the gluon-fusion contribution is still a significant fraction and therefore, the correct estimate would require simulation of the kinematics of $gg \rightarrow R(H) + 2$ jets to high accuracy as well as full detector simulation. A possible way out is to use the gg -fusion subtracted numbers as have been reported by ATLAS. However, to extract this contribution the ATLAS analysis uses the estimate of gluon fusion production for SM higgs as a background which requires, by definition, to assume the SM. We have therefore neglected the VBF mode in our study.

Another important effect arises when the mass of both the scalar eigenstates is close to each other. In such cases, the interference effects cannot be neglected. We have therefore calculated the full interference effects when $122 < m_R < 127$ GeV. As we shall see in the next section, this has important effects both on exclusions as well as on the global best-fit regions.

In addition, there is the possibility that the branching ratio for the decay $\varphi' \rightarrow h'h'$ can be substantial in certain regions of the parameter space, resulting in an enhancement even in fully reconstructible channels. Such signals are relatively suppressed for the $WW^{(*)}$ channel because of various vetos on additional leptons and jets. However they contribute to the $ZZ^{(*)}$ and $\gamma\gamma$ channels where the analysis is by and large inclusive. We have included this kind of processes whenever the resultant enhancement is more than 5% of the direct production rate i.e. $\sigma(pp \rightarrow \varphi') \times B(\varphi' \rightarrow h'h') \geq 0.05\sigma(pp \rightarrow h')$ for the sake of completeness.

We end this subsection by reiterating the parameters used in our scan. They are Λ_φ, ξ and mass of either of the mixed radion state m_R (or the mixed higgs state m_H), with the other fixed at 125 GeV. We use four representative values of Λ_φ , namely 1.5 TeV, 3 TeV,

Channel	ATLAS	CMS	Tevatron
WW^*	1.0 ± 0.3	0.68 ± 0.20	
ZZ^*	1.5 ± 0.4	0.92 ± 0.28	
$\gamma\gamma$	1.6 ± 0.3	0.77 ± 0.27	
$\tau\tau$	0.8 ± 0.7	1.10 ± 0.41	
$b\bar{b}$ (Tevatron)			1.97 ± 0.71

Table 1. Best-fit values of signal strength used for global fits [60–62].

5 TeV and 10 TeV. ξ is varied over the entire theoretically allowed region according to the criteria discussed earlier.

3.2 Allowed regions of the parameter space

First, we remember that the experiments have provided 95% upper limits on the signal strength in each channel, which can be used to rule out regions of our parameter space incompatible with observed data. For the $\gamma\gamma$ and $ZZ^{(*)}$ channel-based exclusions, we make use of the simplified formula given in (Eqn. 3.3) for the entire range of m_R .

The case for $WW^{(*)}$ is more complicated in the region where m_R lies in the range 110 - 160 GeV since contribution from both the eigenstates are of comparable magnitude. Therefore, we add the contributions from both states (Eqn. 3.4). For example, for calculating the cross section at say 150 GeV, we consider the contribution from $m_R = 150$ GeV as well as the contribution from $m_H = 125$ GeV to cuts designed for the 150 GeV analysis. As m_R approaches 160 GeV, the contribution from the 125 GeV state becomes smaller and smaller till after 160, it is dominated entirely by m_R . After this point, we continue with the simple ratio treatment viz.

$$\mu(125; WW) = \frac{\text{B}(R \rightarrow WW)\text{B}(R \rightarrow gg)}{\text{B}(h_{SM} \rightarrow WW)\text{B}(h \rightarrow gg)} \quad (3.5)$$

A second source of upper limits comes from demanding that the total signal strength at 125 GeV does not exceed the upper limit at that mass. The cuts based on transverse mass e.g. the ATLAS cut on transverse mass demanding $0.75m_H < m_T < m_H$ cuts off part of the contribution from m_R state.

$$\mu(WW) = p_{gg}^H \frac{\text{B}(H \rightarrow WW)}{\text{B}(h_{SM} \rightarrow WW)} + p_{gg}^R \frac{a(125; R)}{a(125; h_{SM})} \frac{\text{B}(R \rightarrow WW)}{\text{B}(h_{SM} \rightarrow WW)} \quad (3.6)$$

In the ATLAS analysis, the kinematical cuts for higgs search up to mass of 200 GeV are identical excepting the transeverse mass cut. In the CMS analysis, the cuts vary continuously with mass. We refer the reader to the relevant papers [57–59] for details of the cuts used.

3.3 Best fit contours

To answer the second question posed at the begining of Sec. 3.1, we wish to obtain the best fit values for ξ and the varying scalar mass (m_R or m_H) for each value of Λ_ϕ . We primarily

use data in the $\gamma\gamma$, $ZZ^{(*)}$ and $WW^{(*)}$ channels, which are the most robust. We also use $\tau\bar{\tau}$ data, however, we find that the error bars for these are so large its role in deciding the favoured region of the parameter space is somewhat inconsequential. For the $b\bar{b}$ final state, we use data in the associated production channels WH, ZH [62]. We do not use the data from LHC in this channel as its error bars are larger even than the $\tau\bar{\tau}$ channel and therefore do not restrict any of the parameter space.

To find the best fit, our task is to scan the parameter space and find the values of $m_{\phi'}$ and ξ for any Λ_ϕ , which minimise

$$\chi^2 = \sum_i \frac{(\mu_i - \hat{\mu}_i)^2}{\bar{\sigma}_i^2} \quad (3.7)$$

where $\mu_i = \sigma/\sigma_{SM}$ is the signal strength at 125 GeV as calculated in the i th channel, $\hat{\mu}_i$ denotes the experimental best fit value for that channel, and $\bar{\sigma}_i$ being the corresponding standard deviation. Changing ξ and m_R affect the signal strength of H even though m_H is held fixed at 125 GeV. Again, we use the simple ratio-based formulae for $\gamma\gamma$, $ZZ^{(*)}$, $b\bar{b}$ and $\tau\bar{\tau}$ (using associated production instead of gluon fusion for $b\bar{b}$). For $WW^{(*)}$, the formula (Eqn. 3.6) is used. The data points used for performing global fit are summarised in Table 1.

The 68% and 95 % contours are determined using

$$\chi^2 = \chi_{min}^2 + \Delta\chi^2 \quad (3.8)$$

where $\Delta\chi^2$ values corresponding to the confidence levels for seven degrees of freedom (8.15, 14.1) are used. Since the best-fit values reported by the experiments are based on combination of 7 and 8 TeV runs, we combine our signal strengths at 7 and 8 TeV weighted by the luminosity.

Since the upper limits are based on signal strength mainly due to the second resonance whereas the best-fit requires the correct signal strength at 125 GeV, there may be regions with a small chi-squared that are already ruled out due to constraints on signal from the second resonance. We therefore also perform the best fit in the region left out after the exclusion limits are applied. However, to avoid overconstraining the parameter space, we do not include the exclusions arising from upper limit on the signal strength at 125 GeV as given by (Eqn. 3.6) while performing the chi-squared minimisation.

4 Results and discussions

The most recent CMS and ATLAS search results exclude the Standard Model higgs in the mass range 128 to 600 GeV at 95% CL [60, 61]. In this section we present the regions of the RS parameter space that allow the presence of an extra scalar consistent with observed upper limits.

We illustrate the effect of taking signal contributions from both states in Fig. 1. The top-left panel shows the excluded region when the upper limits are placed on signal strength of the extra R state alone using only the multiplicative correction of Eqn. 3.3. This was

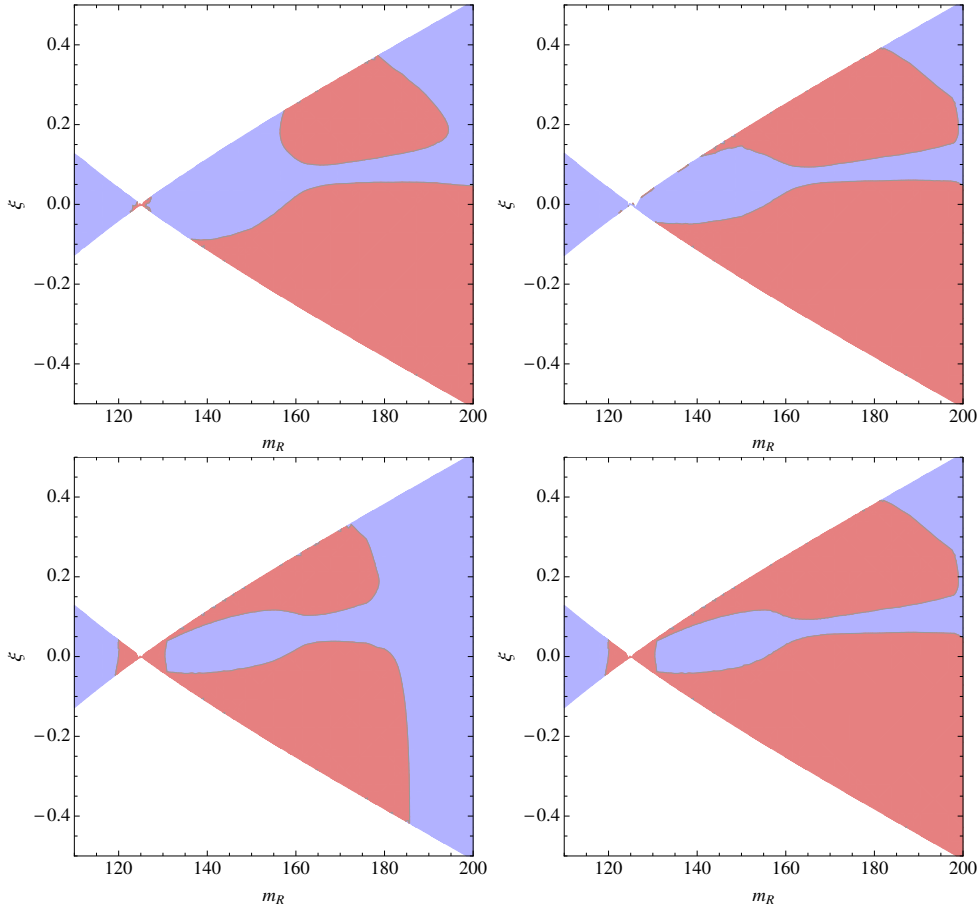


Figure 1. The effect on the excluded parameter space (shown in red) from various contributions. The top-left panel shows the excluded region using ratios of branching fractions of m_R alone. The top-right panel is the exclusion when contribution from both states are taken into account. The bottom-left panel shows the exclusion from applying the limit on signal strength at 125 GeV. Finally, the bottom-right panel shows the total excluded parameter space. This illustration uses $\Lambda_\varphi = 3$ TeV and 95% CL limits from the ATLAS collaboration.

the approach used e.g. in [37]. However, the presence of two states means there are two sources of limits — firstly, we require the total signal strength at 125 GeV to be less than the observed upper limit at 125 GeV (bottom-left panel) and secondly, we also require that the combined signal strength be smaller than the observed limit at the mass of the radion-like resonance m_R (top-right panel). Finally we show the effects of both these taken together to give the full exclusion (bottom-right panel).

A caveat in the above result is that the likelihood function used by the experiments to place limits makes use of not just on the total number of events but also the shape of certain distributions like the lepton invariant mass $m_{\ell\ell}$ or the transverse mass m_T .²

²The transverse mass variable is defined as $m_T = \sqrt{(E_T^{\ell\ell} + E_T^{miss})^2 - |(p_T^{\ell\ell} + E_T^{miss})|^2}$, where $E_T^{\ell\ell}$ is the transverse energy of the leptonic system, $p_T^{\ell\ell}$ is the total transverse momentum of the leptonic system and E_T^{miss} is the missing energy.

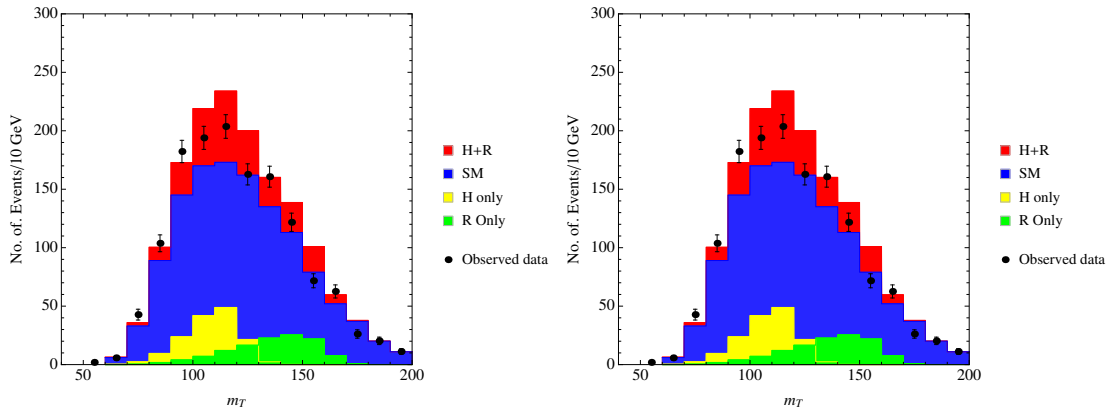


Figure 2. Comparison of m_T distribution after contribution from both scalars is taken into account for a parameter point that is ruled out and one that is not by the ATLAS limits. The parameters for illustration are $\xi = 0.045$ (left; disallowed) and $\xi = 0.065$ (right; allowed), $m_H = 125$ GeV, $m_R = 164$ GeV and $\Lambda_\varphi = 3$ TeV. The label “SM” refers to the total SM background as extracted from [57, 59].

The presence of a shoulder, in e.g. the m_T distribution, can be indicative of a second state and could possibly lead to stronger exclusions in the region where $m_R > m_H$. For a fixed ξ , the branching fraction $R \rightarrow WW^*$ reaches its maximum value for about 160 GeV. For masses greater than this threshold, the change in total signal strength is governed mainly by the change in the production cross section. However, since the production cross section decreases with increasing m_R , the distortion in m_T distribution from the extra state also becomes smaller with increasing m_R and is maximal around 160 GeV.

We present the m_T distribution showing extra contribution from R for $m_R = 164$ GeV in Fig. 2 for two nearby values of ξ viz. 0.045 and 0.065. Our calculation of the m_T distribution is superimposed over the estimated background reported by ATLAS [57]. There are in principle, regions of parameter space where the contribution at 125 GeV from R even exceeds that from H . However, we find that the current upper limits on signal strength in WW channel are so strong that this always results in a very large total signal strength at m_R and is consequently ruled out. This is illustrated in Fig. 2 where the point with $\xi = 0.045$ shows a significant contribution from R but we find it is already disallowed by the 95% upper limits on signal strength at 164 GeV.

This observation justifies our assumption that the distortion in the m_T distribution is not too large even for $m_R \gtrsim 160$ GeV. We therefore present our results with the assumption that the upper limits on total signal strength give a reasonably good approximation of the true exclusion limits even though in principle it corresponds to a limit on the overall normalisation of the distribution only.

4.1 Exclusion of the Parameter Space

We show the regions of parameter space ruled out from current ATLAS and CMS data in Fig. 3. As expected, the allowed parameter space for low Λ_φ is more restricted than for higher values. We find that barring a small sliver close to $\xi = 0$, almost the entire

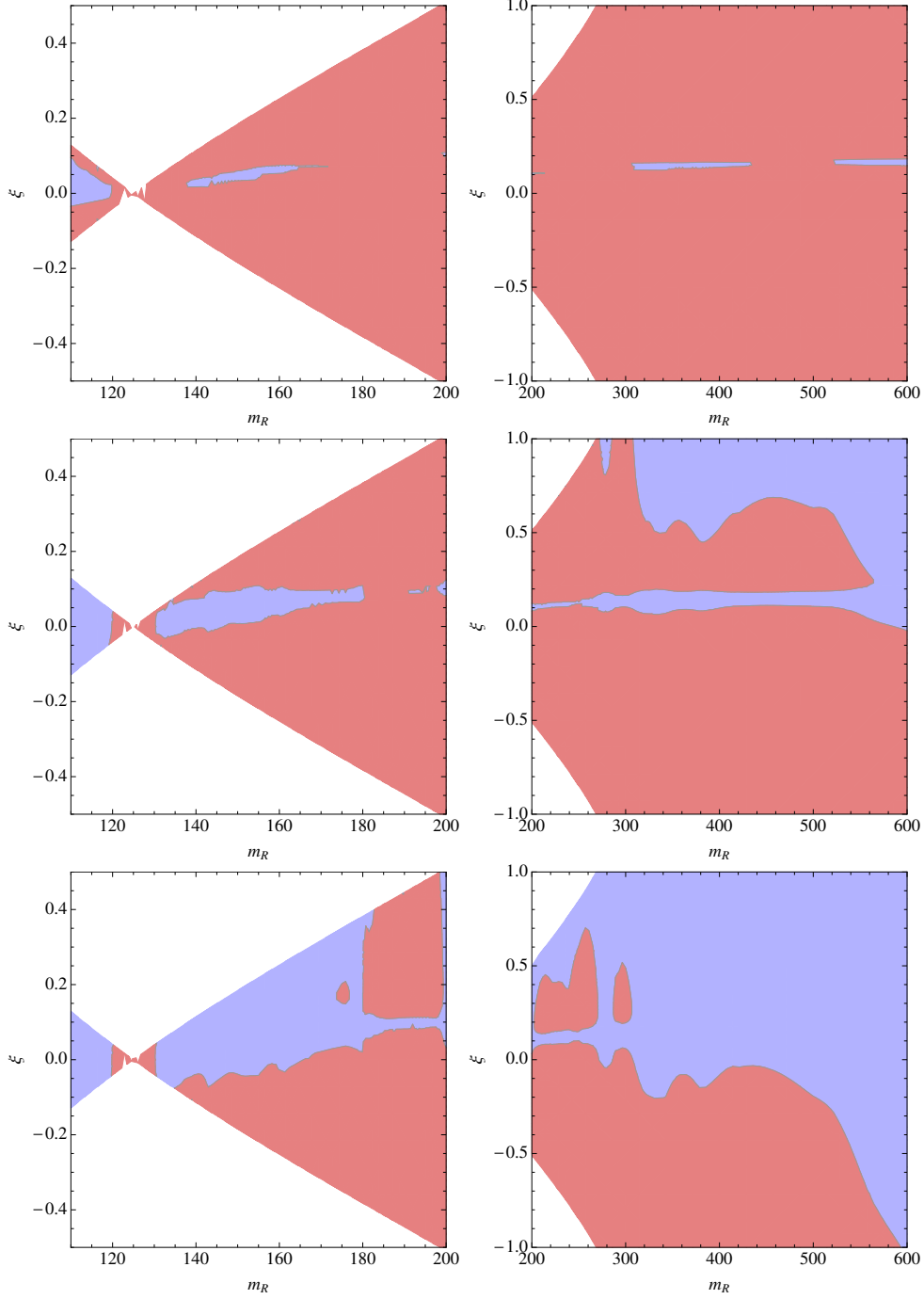


Figure 3. Excluded parameter space for the case with $m_H = 125$ GeV (shown in red) using 95% CL limits from the ATLAS and CMS. This illustration uses $\Lambda_\varphi = 1.5$ TeV(top), 3 TeV(mid) and 5 TeV(bottom).

parameter space is ruled out for $\Lambda_\varphi = 1.5$ TeV. For $\Lambda_\varphi = 3, 5$ TeV, the exclusion is less severe. However, the region with nearly degenerate R and H states is ruled out. At large

m_R , the most stringent limits come from ZZ . We therefore find regions where a significant branching fraction $R \rightarrow t\bar{t}$ reduces the constraints after $m_R > 350$ GeV. However limits are still restrictive for negative ξ values as the production via gluon fusion is enhanced in this region.

We also find that CMS constraints are much stronger than ATLAS. This is expected in $WW^{(*)}$ since CMS has provided limits based on the full 7 and 8 TeV dataset whereas ATLAS has provided only partial results [57, 58]. We list here the corresponding conference notes from ATLAS that have been used for determining the ATLAS limits. Both experiments give limits in ZZ channel based on the full dataset [63, 64].

The $\gamma\gamma$ limits are available only in the range 110-150 GeV [65, 66], presumably since the SM higgs decays into the diphoton channel becomes negligibly small beyond this range. However, since there can be enhancements to this rate in the radion-higgs mixed scenario, it may be useful to have the limits in the full range. Taking interference of both states when their masses lie between 122 and 127 GeV pushes the predicted signal strength beyond the observed upper limits thus ruling out the degenerate region entirely. The $b\bar{b}$ limits, from ATLAS, CMS or Tevatron are found to not affect the extent of the region of exclusion.

Whenever the limits are based on combined datasets, we combine our calculated signal strength at 7 and 8 TeV with the luminosities serving as weights. For $\Lambda_\varphi = 10$ TeV, we do not find any significant exclusions.

A natural question to follow this analysis is what happens if the boson found at 125 GeV is the m_R state and not the m_H one. The exclusions resulting from reversing our analysis in accord with this change is shown in Fig. 4. We find here that larger values of Λ_φ have larger exclusions with almost the entire parameter space being excluded for $\Lambda_\varphi > 5$ TeV. This is in accordance with [28] where they show that a pure radion at 125 GeV is already ruled out. As Λ_φ increases, H becomes more and more like the SM higgs (and equivalently R becomes a pure radion). As the limits on SM higgs already rule it out in most of the mass range, we find that nearly the entire parameter space is ruled out too. In performing the reverse analysis, we have not considered the interference from both states, therefore the small allowed region near 125 GeV should be taken with a pinch of salt. Since the result should not change from the earlier case as $m_R \simeq m_H$ in this region and we may assume that it will be ruled out if a full calculation with interference is made.

4.2 Regions of best-fit with the data

Using the chi-squared analysis outlined in the Sec. 3.3, we perform a global fit using the values of signal strength shown in Table 1. We also perform the same exercise after removing the regions excluded by the upper limits. Of course, while doing so, we do not apply the upper limit on signal strength at 125 GeV. So the only exclusions considered are those resulting from limits on signal from m_R only. For illustration, we show the results at $\Lambda_\varphi = 3$ TeV in Fig. 5. The first panel shows the regions that agree with the data within 68% and 95%. The second panel shows the reduction in the best-fit region when the exclusions reported in Fig. 4 are imposed as well. The bottom panel shows the best-fit region after exclusions for the reverse case where $m_R = 125$ GeV and m_H is varied.

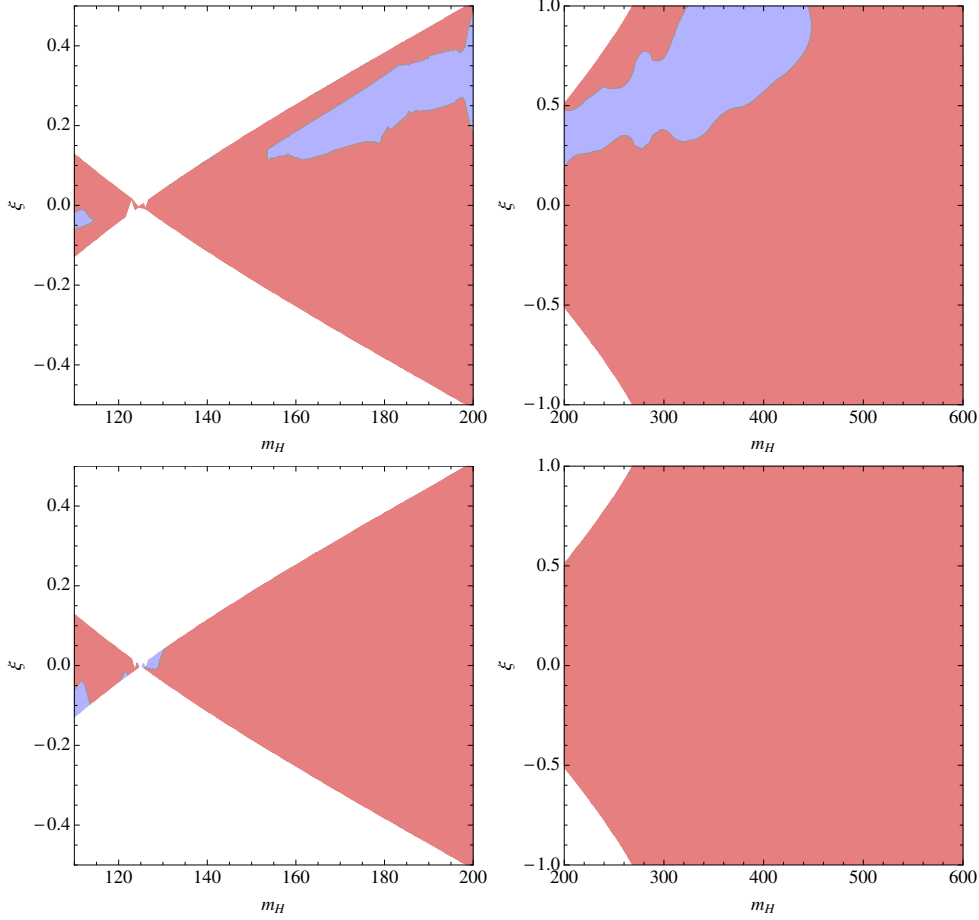


Figure 4. Excluded parameter space (shown in red) for the case with $m_R = 125$ GeV using 95% CL limits from the ATLAS and CMS. This illustration uses $\Lambda_\varphi = 1.5$ TeV (top) and 3 TeV (bottom). Almost the entire parameter space is excluded for $\Lambda_\varphi = 5$ TeV and higher.

The chi-squared value for the SM is 10.93 for nine degrees of freedom. We find that in the first case with $m_H = 125$ GeV, there is always a small region of parameter space that fits with a similar χ^2/dof as the SM. For $\Lambda_\varphi = 1.5$ TeV, the minimum chi-squared value found is 9.06 without exclusions and 11.57 with exclusions at point $m_R = 600$ GeV and $\xi = 0.15$ (after excl.). For 3 TeV, the numbers are (9.03, 9.08) respectively with the best-fit point at $m_R = 407$ GeV and $\xi = 0.15$ and for 5 TeV, they are (9.03, 9.04) with the best-fit point at $m_R = 383$ GeV and $\xi = -0.25$. Thus, the exclusions affect less and less as we increase Λ_φ , which is expected as the excluded parameter space also reduces. In particular, as the exclusions on negative ξ are relaxed, these values seem to give a slightly better fit. Although, as seen from the change in χ^2 with and without exclusion, the distribution is rather flat for large m_R . Also, as the best-fit value for m_R is at the edge of our scan for $\Lambda_\varphi = 1.5$ TeV, it is possible that the fit would be further improved by increasing m_R . For larger values of Λ_φ however, increasing m_R seems to increase the χ^2/dof slightly.

The chi-squared for the reverse case is decidedly worse than in the normal case. We

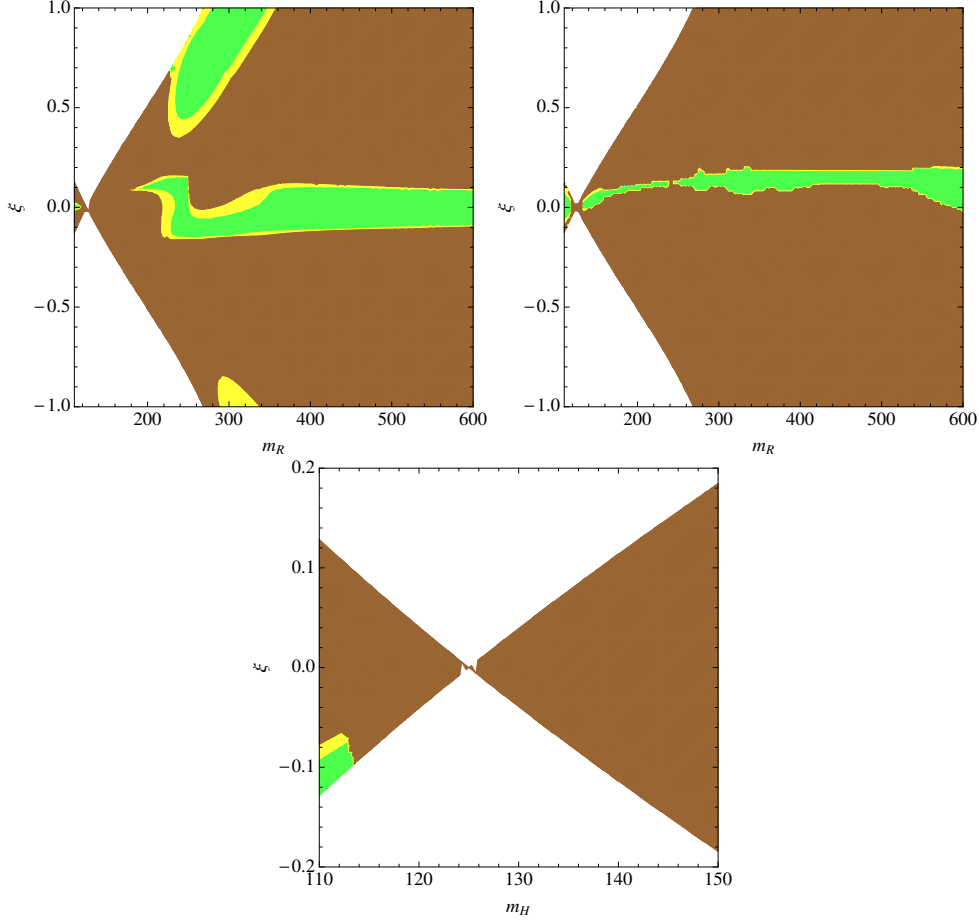


Figure 5. Regions that agree with current data within 68% (green) and 95.4% (yellow) for $\Lambda_\varphi = 3$ TeV. The top-left plot shows the case where no exclusions have been taken into account. The top-right side shows the change after taking exclusions into account. The bottom plot is for the case where we hold $m_R = 125$ GeV instead of m_H .

find that the minimum values of chi-squared after exclusions are 35.6, 18.22, 52.0 for (1.5, 3, 5 TeV). Therefore, we can say that this scenario is strongly disfavoured compared to the SM.

5 Conclusions

We have examined the possibility that the currently observed scalar is one of the two states of a mixed radion-higgs scenario. To perform this analysis, we have considered the contribution from both states in the $WW^{(*)}$ channel, differently affected by cuts, to calculate the signal strength. We also take into account effects of interference when both states are nearly degenerate.

We find that if the 125 GeV state is radion-dominated, only a very small region of the parameter space with a small Λ_φ is consistent with current upper limits. Even in these

regions, the goodness of fit with data is decidedly worse than in the SM. Therefore, we may conclude that the idea that the discovered boson at 125 GeV is dominantly radion-like is largely disfavoured.

The second possibility, namely that the LHC has found a 125 GeV higgs-dominated scalar, but a radion-dominated state, too, hangs around to contribute to the observed signals (especially the $WW^{(*)}$ signal), can not be ruled out with current data. We find the scenario with small (but non-zero) mixing and an accompanying radion-dominated state with high mass results in a good fit for almost all values of Λ_φ . However, if we include exclusions on the presence of the second, radion-dominated boson that would surely accompany the higgs-dominated state, the goodness of fit is reduced for TeV-range values of Λ_φ . We find that for Λ_φ up to 5 TeV, the SM still provides a better fit. As a special case, we find that situations where the two mass eigenstates are degenerate enough to warrant the inclusion of interference terms, are ruled out. Finally $\Lambda_\varphi = 10$ TeV is mostly indistinguishable from the SM as the modifications to signal strengths are too small to be significant.

6 Acknowledgements

We would like to thank Soumitra SenGupta for helpful discussions. UM would like to thank Taushif Ahmed, Shankha Banerjee, Atri Bhattacharya, Nabarun Chakraborty, Ujjal Kumar Dey, Anushree Ghosh, Sourav Mitra, Manoj Mandal, Tanumoy Mandal and Saurabh Niyogi for discussions and assistance. We would also like to thank the Indian Association for the Cultivation of Science, Kolkata for hospitality while this study was in progress. ND is supported partly by the London Centre for Terauniverse Studies (LCTS), using funding from the European Research Council via the Advanced Investigator Grant 267352. UM and BM are partially supported by funding available from the Department of Atomic Energy, Government of India for the Regional centre for Accelerator-based Particle Physics, Harish-Chandra Research Institute. Computational work for this study was partially carried out at the cluster computing facility in the Harish Chandra Research Institute (<http://cluster.hri.res.in>).

References

- [1] **ATLAS Collaboration** Collaboration, G. Aad et al., *Observation of a new particle in the search for the Standard Model Higgs boson with the ATLAS detector at the LHC*, *Phys.Lett.* **B716** (2012) 1–29, [[arXiv:1207.7214](https://arxiv.org/abs/1207.7214)].
- [2] **CMS Collaboration** Collaboration, S. Chatrchyan et al., *Observation of a new boson at a mass of 125 GeV with the CMS experiment at the LHC*, *Phys.Lett.* **B716** (2012) 30–61, [[arXiv:1207.7235](https://arxiv.org/abs/1207.7235)].
- [3] L. Randall and R. Sundrum, *A Large mass hierarchy from a small extra dimension*, *Phys.Rev.Lett.* **83** (1999) 3370–3373, [[hep-ph/9905221](https://arxiv.org/abs/hep-ph/9905221)].
- [4] H. Davoudiasl, J. Hewett, and T. Rizzo, *Phenomenology of the Randall-Sundrum Gauge Hierarchy Model*, *Phys.Rev.Lett.* **84** (2000) 2080, [[hep-ph/9909255](https://arxiv.org/abs/hep-ph/9909255)].

- [5] H. Davoudiasl, J. Hewett, and T. Rizzo, *Experimental probes of localized gravity: On and off the wall*, *Phys.Rev.* **D63** (2001) 075004, [[hep-ph/0006041](#)].
- [6] S. Chang and M. Yamaguchi, *Fate of gravitons in warped extra dimension*, [hep-ph/9909523](#).
- [7] *Search for high-mass dilepton resonances in 20 fb⁻¹ of pp collisions at $\sqrt{s} = 8$ tev with the atlas experiment*, Tech. Rep. ATLAS-CONF-2013-017, CERN, Geneva, Mar, 2013.
- [8] **CMS Collaboration** Collaboration, S. Chatrchyan et al., *Search for narrow resonances using the dijet mass spectrum in pp collisions at $\sqrt{s} = 8$ TeV*, [arXiv:1302.4794](#).
- [9] W. D. Goldberger and M. B. Wise, *Modulus stabilization with bulk fields*, *Phys.Rev.Lett.* **83** (1999) 4922–4925, [[hep-ph/9907447](#)].
- [10] W. D. Goldberger and M. B. Wise, *Phenomenology of a stabilized modulus*, *Phys.Lett.* **B475** (2000) 275–279, [[hep-ph/9911457](#)].
- [11] G. F. Giudice, R. Rattazzi, and J. D. Wells, *Graviscalars from higher dimensional metrics and curvature Higgs mixing*, *Nucl.Phys.* **B595** (2001) 250–276, [[hep-ph/0002178](#)].
- [12] C. Csaki, M. L. Graesser, and G. D. Kribs, *Radion dynamics and electroweak physics*, *Phys.Rev.* **D63** (2001) 065002, [[hep-th/0008151](#)].
- [13] C. Csaki, M. Graesser, L. Randall, and J. Terning, *Cosmology of brane models with radion stabilization*, *Phys.Rev.* **D62** (2000) 045015, [[hep-ph/9911406](#)].
- [14] D. Dominici, B. Grzadkowski, J. F. Gunion, and M. Toharia, *The Scalar sector of the Randall-Sundrum model*, *Nucl.Phys.* **B671** (2003) 243–292, [[hep-ph/0206192](#)].
- [15] C. Csaki, J. Hubisz, and S. J. Lee, *Radion phenomenology in realistic warped space models*, *Phys.Rev.* **D76** (2007) 125015, [[arXiv:0705.3844](#)].
- [16] U. Mahanta and S. Rakshit, *Some low-energy effects of a light stabilized radion in the Randall-Sundrum model*, *Phys.Lett.* **B480** (2000) 176–180, [[hep-ph/0002049](#)].
- [17] J. F. Gunion, M. Toharia, and J. D. Wells, *Precision electroweak data and the mixed Radion-Higgs sector of warped extra dimensions*, *Phys.Lett.* **B585** (2004) 295–306, [[hep-ph/0311219](#)].
- [18] M. Toharia, *Precision electroweak constraints on the mixed radion Higgs sector*, [hep-ph/0402092](#).
- [19] M. Toharia, *Higgs-Radion Mixing with Enhanced Di-Photon Signal*, *Phys.Rev.* **D79** (2009) 015009, [[arXiv:0809.5245](#)].
- [20] M. Frank, B. Korutlu, and M. Toharia, *Saving the fourth generation Higgs with radion mixing*, *Phys.Rev.* **D85** (2012) 115025, [[arXiv:1204.5944](#)].
- [21] T. G. Rizzo, *Effects on Higgs boson properties from radion mixing*, [hep-ph/0207113](#).
- [22] K. Cheung, C. Kim, and J. Song, *Probing the radion-Higgs mixing at photon colliders*, *Phys.Rev.* **D72** (2005) 115015, [[hep-ph/0509017](#)].
- [23] T. Han, G. D. Kribs, and B. McElrath, *Radion effects on unitarity in gauge boson scattering*, *Phys.Rev.* **D64** (2001) 076003, [[hep-ph/0104074](#)].
- [24] M. Chaichian, A. Datta, K. Huitu, and Z.-h. Yu, *Radion and Higgs mixing at the LHC*, *Phys.Lett.* **B524** (2002) 161–169, [[hep-ph/0110035](#)].

- [25] M. Battaglia, S. De Curtis, A. De Roeck, D. Dominici, and J. F. Gunion, *On the complementarity of Higgs and radion searches at LHC*, *Phys.Lett.* **B568** (2003) 92–102, [[hep-ph/0304245](#)].
- [26] B. Bhattacharjee and S. Raychaudhuri, *Tevatron Signal for an Unmixed Radion*, [arXiv:1104.4749](#).
- [27] V. Goncalves and W. Sauter, *Radion production in exclusive processes at CERN LHC*, *Phys.Rev.* **D82** (2010) 056009, [[arXiv:1007.5487](#)].
- [28] V. Barger, M. Ishida, and W.-Y. Keung, *Differentiating the Higgs boson from the dilaton and the radion at hadron colliders*, *Phys.Rev.Lett.* **108** (2012) 101802, [[arXiv:1111.4473](#)].
- [29] K. Cheung and T.-C. Yuan, *Could the excess seen at 124-126 GeV be due to the Randall-Sundrum Radion?*, *Phys.Rev.Lett.* **108** (2012) 141602, [[arXiv:1112.4146](#)].
- [30] H. Davoudiasl, T. McElmurry, and A. Soni, *The Radion as a Harbinger of Deca-TeV Physics*, *Phys.Rev.* **D86** (2012) 075026, [[arXiv:1206.4062](#)].
- [31] I. Low, J. Lykken, and G. Shaughnessy, *Have We Observed the Higgs (Imposter)?*, *Phys.Rev.* **D86** (2012) 093012, [[arXiv:1207.1093](#)].
- [32] D. Soa, T. Tham, N. Thao, D. Thuy, D. Thuy, et al., *Radion production in gamma-electron collisions*, *Mod.Phys.Lett.* **A27** (2012) 1250126, [[arXiv:1207.6471](#)].
- [33] Z. Chacko, R. Franceschini, and R. K. Mishra, *Resonance at 125 GeV: Higgs or Dilaton/Radion?*, *JHEP* **1304** (2013) 015, [[arXiv:1209.3259](#)].
- [34] V. Barger and M. Ishida, *Randall-Sundrum Reality at the LHC*, *Phys.Lett.* **B709** (2012) 185–191, [[arXiv:1110.6452](#)].
- [35] B. Grzadkowski, J. F. Gunion, and M. Toharia, *Higgs-Radion interpretation of the LHC data?*, *Phys.Lett.* **B712** (2012) 70–80, [[arXiv:1202.5017](#)].
- [36] H. de Sandes and R. Rosenfeld, *Radion-Higgs mixing effects on bounds from LHC Higgs Searches*, *Phys.Rev.* **D85** (2012) 053003, [[arXiv:1111.2006](#)].
- [37] H. Kubota and M. Nojiri, *Radion-higgs mixing state at the LHC with the KK contributions to the production and decay*, [arXiv:1207.0621](#).
- [38] Y. Ohno and G.-C. Cho, *Production and decay of a heavy radion in Randall-Sundrum model at the LHC*, *EPJ Web Conf.* **49** (2013) 18003, [[arXiv:1301.7514](#)].
- [39] G.-C. Cho, D. Nomura, and Y. Ohno, *Constraints on radion in a warped extra dimension model from Higgs boson searches at the LHC*, [arXiv:1305.4431](#).
- [40] W. D. Goldberger and M. B. Wise, *Bulk fields in the Randall-Sundrum compactification scenario*, *Phys.Rev.* **D60** (1999) 107505, [[hep-ph/9907218](#)].
- [41] H. Davoudiasl, J. Hewett, and T. Rizzo, *Bulk gauge fields in the Randall-Sundrum model*, *Phys.Lett.* **B473** (2000) 43–49, [[hep-ph/9911262](#)].
- [42] A. Pomarol, *Gauge bosons in a five-dimensional theory with localized gravity*, *Phys.Lett.* **B486** (2000) 153–157, [[hep-ph/9911294](#)].
- [43] K. Agashe, A. Belyaev, T. Krupovnickas, G. Perez, and J. Virzi, *LHC Signals from Warped Extra Dimensions*, *Phys.Rev.* **D77** (2008) 015003, [[hep-ph/0612015](#)].
- [44] K. Agashe, G. Perez, and A. Soni, *B-factory signals for a warped extra dimension*, *Phys.Rev.Lett.* **93** (2004) 201804, [[hep-ph/0406101](#)].

- [45] K. Agashe, G. Perez, and A. Soni, *Flavor structure of warped extra dimension models*, *Phys.Rev.* **D71** (2005) 016002, [[hep-ph/0408134](#)].
- [46] K. Agashe, A. Delgado, M. J. May, and R. Sundrum, *RS1, custodial isospin and precision tests*, *JHEP* **0308** (2003) 050, [[hep-ph/0308036](#)].
- [47] Y. Tang, *Implications of LHC Searches for Massive Graviton*, *JHEP* **1208** (2012) 078, [[arXiv:1206.6949](#)].
- [48] J. E. Kim, B. Kyae, and H. M. Lee, *Effective Gauss-Bonnet interaction in Randall-Sundrum compactification*, *Phys.Rev.* **D62** (2000) 045013, [[hep-ph/9912344](#)].
- [49] J. E. Kim, B. Kyae, and H. M. Lee, *Various modified solutions of the Randall-Sundrum model with the Gauss-Bonnet interaction*, *Nucl.Phys.* **B582** (2000) 296–312, [[hep-th/0004005](#)].
- [50] T. G. Rizzo, *Warped phenomenology of higher-derivative gravity*, *JHEP* **0501** (2005) 028, [[hep-ph/0412087](#)].
- [51] S. Choudhury and S. Sengupta, *Features of warped geometry in presence of Gauss-Bonnet coupling*, *JHEP* **1302** (2013) 136, [[arXiv:1301.0918](#)].
- [52] U. Maitra, B. Mukhopadhyaya, and S. SenGupta, *Reconciling small radion vacuum expectation values with massive gravitons in an Einstein-Gauss-Bonnet warped geometry scenario*, [arXiv:1307.3018](#).
- [53] T. Sjostrand, S. Mrenna, and P. Z. Skands, *A Brief Introduction to PYTHIA 8.1*, *Comput.Phys.Commun.* **178** (2008) 852–867, [[arXiv:0710.3820](#)].
- [54] J. Alwall, M. Herquet, F. Maltoni, O. Mattelaer, and T. Stelzer, *MadGraph 5 : Going Beyond*, *JHEP* **1106** (2011) 128, [[arXiv:1106.0522](#)].
- [55] **LHC Higgs Cross Section Working Group** Collaboration, S. Dittmaier et al., *Handbook of LHC Higgs Cross Sections: 1. Inclusive Observables*, [arXiv:1101.0593](#).
- [56] A. Denner, S. Heinemeyer, I. Puljak, D. Rebuszi, and M. Spira, *Standard Model Higgs-Boson Branching Ratios with Uncertainties*, *Eur.Phys.J.* **C71** (2011) 1753, [[arXiv:1107.5909](#)].
- [57] **ATLAS Collaboration** Collaboration, G. Aad et al., *Measurements of the properties of the higgs-like boson in the $w^{(*)} \rightarrow \ell\nu\ell\nu$ decay channel with the atlas detector using 25 fb^{-1} of proton-proton collision data*, Tech. Rep. ATLAS-CONF-2013-030, CERN, Geneva, Mar, 2013.
- [58] **CMS Collaboration** Collaboration, S. Chatrchyan et al., *Evidence for a particle decaying to $w+w-$ in the fully leptonic final state in a standard model higgs boson search in pp collisions at the lhc* , Tech. Rep. CMS-PAS-HIG-13-003, CERN, Geneva, 2013.
- [59] **ATLAS Collaboration** Collaboration, G. Aad et al., *Search for the Standard Model Higgs boson in the $H \rightarrow WW^{(*)} \rightarrow \ell\nu\ell\nu$ decay mode with 4.7 /fb of ATLAS data at $\sqrt{s} = 7 \text{ TeV}$* , *Phys.Lett.* **B716** (2012) 62–81, [[arXiv:1206.0756](#)].
- [60] **ATLAS Collaboration** Collaboration, G. Aad et al., *Combined measurements of the mass and signal strength of the higgs-like boson with the atlas detector using up to 25 fb^{-1} of proton-proton collision data*, Tech. Rep. ATLAS-CONF-2013-014, CERN, Geneva, Mar, 2013.
- [61] **CMS Collaboration** Collaboration, S. Chatrchyan et al., *Combination of standard model higgs boson searches and measurements of the properties of the new boson with a mass near 125 gev* , Tech. Rep. CMS-PAS-HIG-13-005, CERN, Geneva, 2013.
- [62] **CDF Collaboration, D0 Collaboration** Collaboration, T. Aaltonen et al., *Evidence for a particle produced in association with weak bosons and decaying to a bottom-antibottom quark*

pair in Higgs boson searches at the Tevatron, *Phys.Rev.Lett.* **109** (2012) 071804, [[arXiv:1207.6436](#)].

- [63] *Properties of the higgs-like boson in the decay h to zz to $4l$ in pp collisions at $\sqrt{s} = 7$ and 8 tev* , Tech. Rep. CMS-PAS-HIG-13-002, CERN, Geneva, 2013.
- [64] *Measurements of the properties of the higgs-like boson in the four lepton decay channel with the atlas detector using 25 fb1 of proton-proton collision data*, Tech. Rep. ATLAS-CONF-2013-013, CERN, Geneva, Mar, 2013.
- [65] *Updated measurements of the higgs boson at 125 gev in the two photon decay channel*, Tech. Rep. CMS-PAS-HIG-13-001, CERN, Geneva, 2013.
- [66] *Observation and study of the higgs boson candidate in the two photon decay channel with the atlas detector at the lhc*, Tech. Rep. ATLAS-CONF-2012-168, CERN, Geneva, Dec, 2012.